Quasi-two-dimensional spin correlations in the triangular lattice bilayer spin glass $LuCoGaO_4$

K. Fritsch,[1,2] K. A. Ross,[2,3] G. E. Granroth,[4] G. Ehlers,[5] H. M. L. Noad,[2,6] H. A. Dabkowska,[7] and B. D. Gaulin[2,7,8]

[1]*Helmholtz Zentrum Berlin für Materialien und Energie GmbH, D-14109 Berlin, Germany*

[2]*Department of Physics and Astronomy, McMaster University, Hamilton, Ontario, L8S 4M1, Canada*

[3]*Colorado State University, Fort Collins, Colorado 80523, USA*

[4]*Neutron Data Analysis and Visualization Division, Oak Ridge National Laboratory, Oak Ridge, Tennessee 37831, USA*

[5]*Quantum Condensed Matter Division, Oak Ridge National Laboratory, Oak Ridge, Tennessee 37831, USA*

[6]*Stanford University, Stanford, California 94305, USA*

[7]*Brockhouse Institute for Materials Research, Hamilton, Ontario, L8S 4M1, Canada*

[8]*Canadian Institute for Advanced Research, 661 University Ave, Toronto, Ontario M5G 1M1, Canada*

(Received 18 April 2017; published 13 September 2017)

We present a single-crystal time-of-flight neutron scattering study of the static and dynamic spin correlations in $LuCoGaO_4$, a quasi-two-dimensional dilute triangular lattice antiferromagnetic spin-glass material. This system is based on Co^{2+} ions that are randomly distributed on triangular bilayers within the $YbFe_2O_4$-type, hexagonal crystal structure. Antiferromagnetic short-range two-dimensional correlations at wave vectors $\mathbf{Q} = (1/3, 1/3, L)$ develop within the bilayers at temperatures as high as $|\Theta_{CW}| \sim 100$ K and extend over roughly five unit cells at temperatures below $T_g = 19$ K. These two-dimensional static correlations are observed as diffuse rods of neutron scattering intensity along c^* and display a continuous spin freezing process in their energy dependence. Aside from exhibiting these typical spin-glass characteristics, this insulating material reveals a novel gapped magnetic resonant spin excitation at $\Delta E \sim 12$ meV localized around $\mathbf{Q} = (1/3, 1/3, L)$. The temperature dependence of the spin gap associated with this two-dimensional excitation correlates with the evolution of the static correlations into the spin-glass state ground state. We associate it with the effect of the staggered exchange field acting on the $S_{eff} = 1/2$ Ising-like doublet of the Co^{2+} moments.

DOI: 10.1103/PhysRevB.96.094414

I. INTRODUCTION

Studies of quasi-two-dimensional frustrated triangular lattice antiferromagnets have been of intense recent research interest due to their exotic low-temperature magnetic properties, embedded within spin-glass or spin-liquid ground states that can arise in these systems [1,2]. Prominent experimental examples for such states based on two-dimensional frustrated triangular geometries include the site-disordered $NiGa_2S_4$ [3], the anisotropic triangular lattice system Cs_2CuCl_4 [4,5], the honeycomb lattice-based system $Ba_3CuSb_2O_9$ [6], and the quantum spin-liquid candidates κ-$(BEDT\text{-}TTF)_2Cu_2(CN)_3$ [7], herbertsmithite [8], and most recently, $YbMgGaO_4$ [9–11].

Here, we present a study of the dilute triangular lattice antiferromagnet bilayer system $LuCoGaO_4$, isostructural to $YbMgGaO_4$, which serves as an important example in which the interplay of site disorder and frustration can be studied. In $LuCoGaO_4$, magnetic frustration is realized by antiferromagnetically coupled Co^{2+} $S_{eff} = 1/2$ Ising magnetic moments on planar triangular bilayers [Figs. 1(a) and 1(b)]. Site disorder arises from the fact that the Co^{2+} ions are statistically distributed in a 1:1 ratio with nonmagnetic Ga^{3+} ions within the bilayers.

$LuCoGaO_4$ belongs to the family of materials with the RFe_2O_4-type structure [Fig. 1(a)] and has the composition $R^{3+}M^{2+}M^{3+}O_4$, in which R is a small rare-earth ion such as Yb^{3+}, Lu^{3+}, or Tm^{3+}, and in which the M^{2+} and M^{3+} ions are $3d$ transition-metal cations such as Fe^{2+}, Fe^{3+}, Mn^{2+}, Mg^{2+}, Cu^{2+}, or Co^{2+} and Ga^{3+}. The M ions can either both be magnetic or can be a mixture of magnetic and nonmagnetic ions (dilute case). In addition, the R ion can also be magnetic or nonmagnetic, leading to complex magnetic and/or charge correlations.

The crystal structure, with space group $R\bar{3}m$, is characterized by transition-metal ions that form double layers of $M^{2+/3+}O_5$ triangular bipyramids, which are connected by triangular layers of RO_6 octahedra, leading to quasi-two-dimensional magnetic properties.

Several combinations of these materials with two different M distributed over the same crystallographic site, and which therefore are expected to display the phenomenology of frustration, have been the focus of previous studies. In addition to $LuCoGaO_4$, $LuCuGaO_4$, $LuMFeO_4$ (M = Zn, Fe, Co, Cu), $YbMFeO_4$ (M = Mg, Fe, Co, Cu), $YbCuGaO_4$, $YbCoGaO_4$ as well as $YbMgGaO_4$ have been studied [9,12–23].

In the series based on the nonmagnetic Lu as R atom, the multiferroic $LuFe_2O_4$ has attracted particular interest due to the observed interplay of cation and magnetic ordering. This material exhibits two- or three-dimensional ferrimagnetic ordering below ~240 K depending on oxygen stoichiometry [24,25], and a charge-ordered state below ~320 K, which is thought to underlie the ferroelectricity [26]. The dilute case has been most extensively investigated for $LuFeMgO_4$ [16–18,20,21,27]. $LuCuGaO_4$ has recently been shown to display spin-liquid behavior with a gapless spin excitation spectrum down to 50 mK [28], in contrast to expectations of spin-glass behavior based on earlier susceptibility measurements [12]. The effects of spin anisotropy on the phase transitions have been investigated and compared for $YbCoGaO_4$ and $LuCoGaO_4$ by Radelytskyi *et al.* [29].

With the exception of $RCuGaO_4$ (R = Yb, Lu) [12,28], all other members of this series exhibit a splitting of field-cooled and zero-field-cooled susceptibilities, however, on very different temperature scales. The majority of these materials shows no indication of magnetic long-range order;

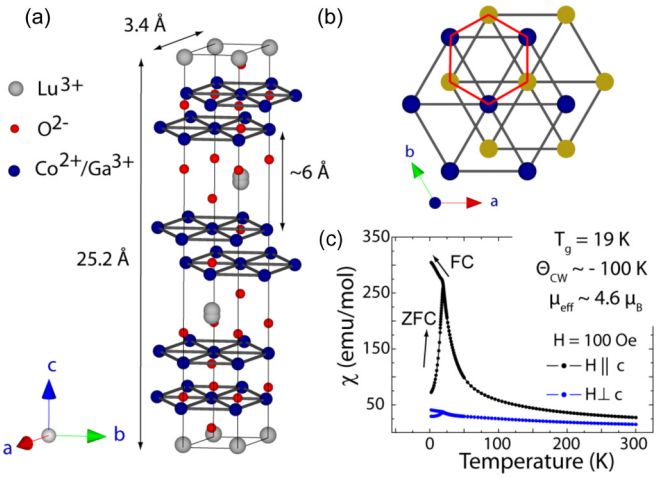

FIG. 1. (a) Crystal structure of $LuCoGaO_4$ showing the rhombohedral unit cell and the planar triangular bilayers in which the $S_{\rm eff} = 1/2$ magnetic moments on the Co^{2+} ions are statistically distributed in a 1:1 ratio with nonmagnetic Ga^{3+} ions. The bilayers in the ab plane are well separated along the c axis by triangular layers composed of nonmagnetic LuO_6 octahedra. (b) The two faces of the bilayer shown in blue and orange as viewed down the c axis. Each face has triangular geometry on which antiferromagnetic interactions will be highly frustrated. The two bilayer faces are staggered such that the shortest bonds form between the cations linking the two faces, thereby forming an undulating honeycomb lattice (shown in red). (c) Magnetic dc susceptibility measured on a single crystal of $LuCoGaO_4$ reveals spin-glass behavior below the freezing temperature $T_g \sim 19$ K.

however, diffuse magnetic scattering has been observed in neutron diffraction studies on (powder) YFe_2O_4 [13], (powder) $LuCuFeO_4$, (powder) $LuZnFeO_4$, (powder and single crystal) $LuFeMgO_4$ [16], and (powder) $LuCuGaO_4$ as a broad peak around $|Q| \sim 1.27$ Å^{-1} at low temperature [28].

The study of this family of materials has been less comprehensive than it otherwise would have been due to the lack of large, high-quality single crystals. We recently succeeded in growing high-quality samples of $LuCoGaO_4$, for which a single-crystal x-ray structural refinement indicates random occupation of the triangular bilayers by Co^{2+} and Ga^{3+} in a 1:1 ratio [30], placing this material at the percolation threshold for triangular lattices of $p_c = 0.5$ [31].

In our single crystal of $LuCoGaO_4$, the splitting of the field-cooled (FC) and zero-field-cooled (ZFC) susceptibilities [see Fig. 1(c)] occurs at $T_g \sim 19$ K, consistent with spin freezing or a spin-glass transition. The determined Curie-Weiss temperature $\Theta_{\rm CW} \sim -100$ K implies antiferromagnetic interactions between the Co^{2+} moments. The paramagnetic moment associated with this Curie-Weiss behavior is 4.6 μ_B, larger than the spin-only 3.87 μ_B expected in the case of quenched angular momentum. The Co^{2+} moment then arises from the appropriate crystal field splitting of the $L = 3$, $S = 3/2$ Hund's rule ground state, which gives a Kramer's doublet corresponding to $S_{\rm eff} = 1/2$ after applying spin-orbit coupling, as is commonly the case in Co^{2+}-based magnetic insulators [32–35].

These results are consistent with previous data from Cava *et al.* obtained on powder samples [12]. The frustration index of $f \sim 5$ indicates moderate frustration. As shown in Fig. 1(c), the susceptibility is anisotropic with a large response for applied fields parallel to the stacking direction of the bilayers along the c axis. Interestingly, a cusp in the ZFC/FC curves is observed for both directions of the applied field, signaling a simultaneous freezing of the longitudinal and transverse spin components. This is in contrast to the behavior displayed by most other members of this family, for example $LuFeMgO_4$ or $LuFeCoO_4$, in which only the longitudinal susceptibility displays freezing [21,27]. It is also different from $YbCoGaO_4$ which is considered an Ising spin glass [29]. It follows that the magnetic nature of the Co^{2+} ions in $LuCoGaO_4$ is Heisenberg-like with relatively strong uniaxial single ion anisotropy, rather than being purely Ising-like in nature. Recent ac-susceptibility measurements [29] also show a frequency dependence for both field directions, and exhibit spin-glass characteristics such as activated behavior in the form of a Vogel-Fulcher law, possible dynamic scaling and a peak shift per decade frequency of ~0.05, consistent with expectations for conventional spin-glass behavior [36].

II. EXPERIMENTAL DETAILS

A large, high-quality single crystal used for neutron scattering measurements was grown at McMaster University using the optical floating zone technique [37]. For the crystal growth, the preannealed starting materials Lu_2O_3 and Ga_2O_3 were first mixed with CoO in the appropriate stoichiometric ratios, then hydrostatically pressed at 60 MPa and the resulting rods were subsequently sintered in air at 1300 °C for 24 hours. The so-obtained polycrystalline rods were used as seed and feed rods in the actual crystal growth, which was performed in a Crystal Systems Inc. floating zone furnace at a growth speed of ~9 mm/hour [30].

Magnetization measurements shown in Fig. 1(c) were performed using a conventional SQUID magnetometer at McMaster University. A small single-crystal sample of mass ~10 mg was cut from the main crystal boule and aligned to within 3° for magnetization measurements with the magnetic field applied parallel or transverse to the plane of the bilayers. The neutron scattering experiments were carried out on a ~10 g single-crystal sample of $LuCoGaO_4$ using the time-of-flight chopper spectrometers SEQUOIA and CNCS at the Spallation Neutron Source of Oak Ridge National Laboratory [38]. The crystal has a mosaicity of 0.75° based on the full-width-half-maxima of the rocking curves on the (0,0,9) and (1,1,0) reflections. The sample was aligned in the (H,H,L) horizontal scattering plane. Measurements on SEQUOIA employed an incident energy of $E_i = 35$ meV, spinning Fermi chopper 1 at 240 Hz and the bandwidth-limiting T_0 chopper at 60 Hz, giving an energy resolution of 1 meV at the elastic line. Data from CNCS were obtained using two settings of the incident energy E_i, 10 meV and 25 meV, resulting in energy resolutions of 0.3 meV and 1.0 meV at the elastic line, respectively. The sample was mounted in a standard Orange cryostat with a base temperature of ~1.5 K. Measurements were collected in step scan mode over a range of 100° at a step size of 1° on SEQUOIA and over a range of 60° at a step size of 3° on CNCS. Both sets of measurements were performed over a wide range of temperatures up to 300 K.

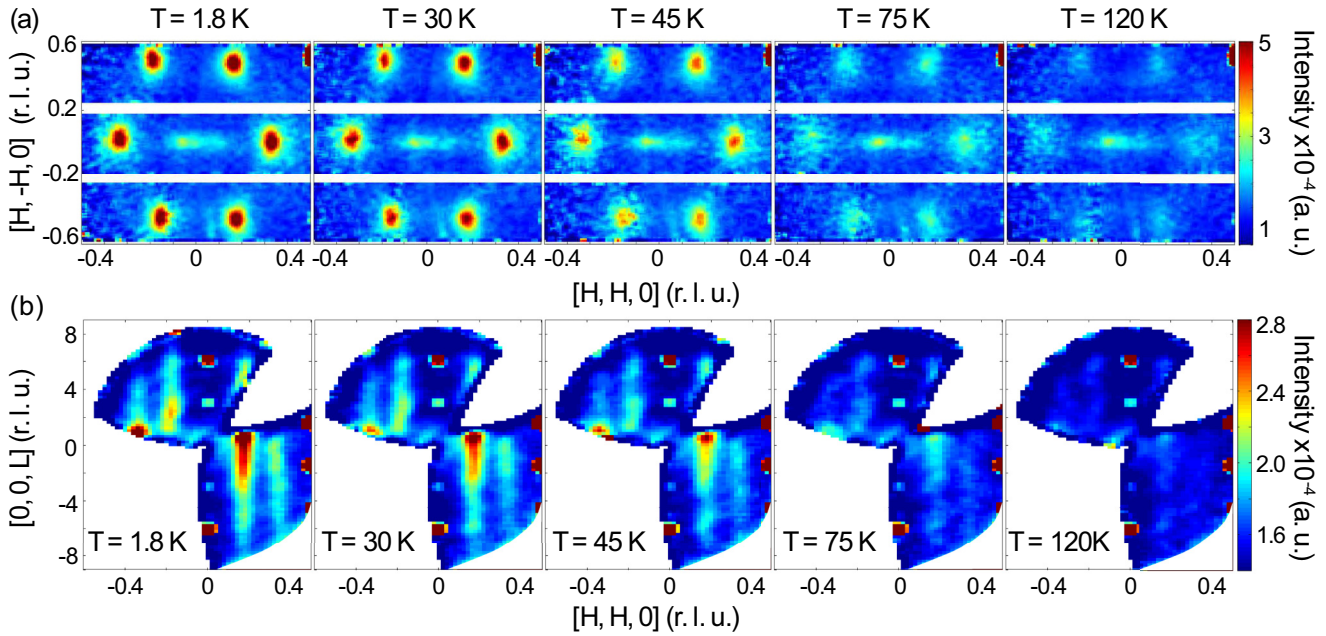

FIG. 2. Elastic scattering maps $S(\mathbf{Q},\hbar\omega = 0)$ as a function of temperature obtained on the fine resolution chopper spectrometer SEQUOIA show the short-range antiferromagnetic spin correlations as diffuse scattering intensity at wave vectors $\mathbf{Q} = (1/3,1/3,L)$ in the plane of the bilayers [(a), top row] and in the plane perpendicular to it [(b), bottom row]. Rods of neutron scattering intensity along the $[0,0,L]$ direction [(b), bottom row] indicate the absence of magnetic correlations along that direction and reveal the two-dimensional character of the magnetic interactions within the bilayer planes. Short-range correlations begin to develop at $T \sim |\Theta_{CW}|$ and gradually evolve into the low-temperature spin-glass phase, without going through a conventional phase transition. The data have been corrected for detector efficiency. The integration ranges for both (a) and (b) are given in the text. Note that the scattering intensity around $\mathbf{Q} = 0$ in (a) is an artifact of the measurement that is observable here as a consequence of the finite binning range along L. This intensity is related to the scattering from the beam stop.

III. STATIC SPIN CORRELATIONS

The static and dynamic correlations in $LuCoGaO_4$ have been studied using the time-of-flight neutron scattering instruments SEQUOIA and CNCS, which allow the simultaneous measurement of the four-dimensional dynamic structure factor $S(\mathbf{Q},\hbar\omega)$ over a large range of reciprocal space in both the horizontal and vertical directions. The evolution of the static correlations with temperature taken with the SEQUOIA spectrometer is shown in Fig. 2.

Figure 2(a), top row, shows the elastic diffuse scattering intensity ($E = [-1,1]$ meV, $[0,0,L] = [-2.75,2.75]$ r.l.u.) within the plane of the bilayers that is clearly observed to be peaked at wave vectors $\mathbf{Q} = (1/3,1/3,L)$. This type of scattering has similarly been observed in several samples of other members of the $YbFe_2O_4$ family [13,16], principally as a broad peak centered at $Q \sim 1.27$ Å^{-1}. Such a feature is typical for antiferromagnetically interacting moments in a triangular geometry and suggests a $\sqrt{3} \times \sqrt{3}$ local magnetic structure. In Fig. 2(b), bottom row, the elastic scattering in the (H,H,L) plane is shown after integrating the data over the vertical $[H,-H,0]$ direction (and in $E = [-1,1]$ meV). Here, the diffuse scattering is observed as rods of scattering, a clear signature of two-dimensional correlations in the a^*-b^* plane perpendicular to the rod direction. The extent of the rodlike scattering along $[0,0,L]$ implies the absence of correlations between bilayers along c^* and therefore confirms the two-dimensional character of this system.

This elastic diffuse scattering is seen to persist up to at least 120 K, showing that a buildup of correlations that will eventually freeze, develops noticeably at temperatures as high as the Curie Weiss temperature ($\Theta_{CW} \sim -100$ K). The isotropic (within the a^*-b^* plane) diffuse scattering profile can be well described by a Ornstein-Zernike (Lorentzian) line shape at all temperatures, and this allows us to extract the correlation length $\xi = 1/\text{HWHM}$ (half-width-half-maximum) in the plane of the bilayers as a function of temperature, as shown in Fig. 3 for both the SEQUOIA and the CNCS data. For the SEQUOIA data, longitudinal, and transverse cuts through the elastic scattering ($E = [-1,1]$ meV) at the six observed peak positions were fit to Lorentzian line shapes. The elastic scattering was integrated along the length of the rod for $[0,0,L] = [-2.75,2.75]$ r.l.u.. The resulting correlation lengths were averaged and these are shown in Fig. 3. For the CNCS data at $E_i = 10$ meV, the elastic scattering intensity ($E = [-0.2,0.2]$ meV) at $(-1/3,-1/3,L)$ was integrated over $[0,0,L] = [-2,2]$ r.l.u. and $[H,-H,0] = [-0.2,0.2]$ r.l.u., while for $E_i = 25$ meV, the scattering intensity was integrated over $E = [-1,1]$ meV, $[0,0,L] = [-0.5,0.5]$, and $[H,-H,0] = [-0.25,0.25]$ r.l.u. at $(1/3,1/3,L)$, and again fit to a Lorentzian line shape to extract the correlation length. The difference in absolute values of the correlation length is a result of the coarser $\mathbf{Q}$ resolution at higher incident energy and of the different binning range in the $[0,0,L]$ direction, which was chosen due to different detector coverages for the two data sets at $E_i = 10$ and 25 meV.

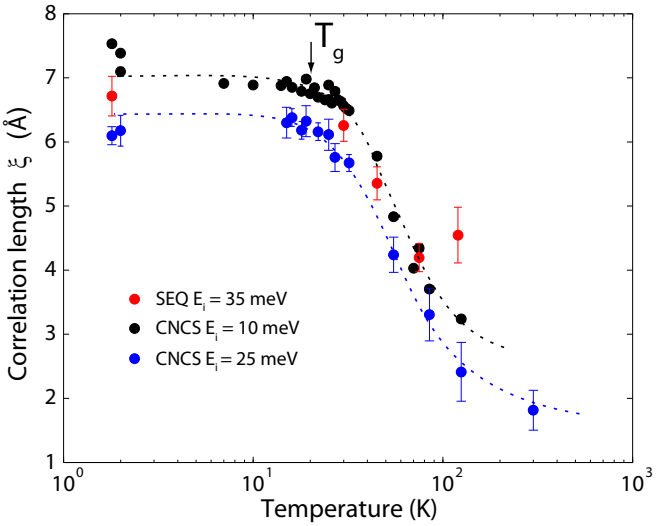

FIG. 3. The correlation length within the plane of the bilayers extracted from cuts through the elastic scattering at $\mathbf{Q} = (1/3,1/3,L)$ for both the SEQUOIA and the CNCS data. The short-range spin correlations gradually develop at temperatures as high as the Curie Weiss temperature at ∼100 K and increase to their maximum value of $\xi \sim 6.5$–7.5 Å below the freezing temperature T_g. There is no sharp anomaly at T_g, in contrast to the observed cusp in the ZFC susceptibility, typical for this family of materials. Note that the difference in absolute values of the correlation length from CNCS data for $E_i = 10$ and 25 meV is a result of the coarser $\mathbf{Q}$ resolution at higher incident energy and a different binning range in L. For details of the integration and fitting, see text. The error bars are $\pm 1\sigma$.

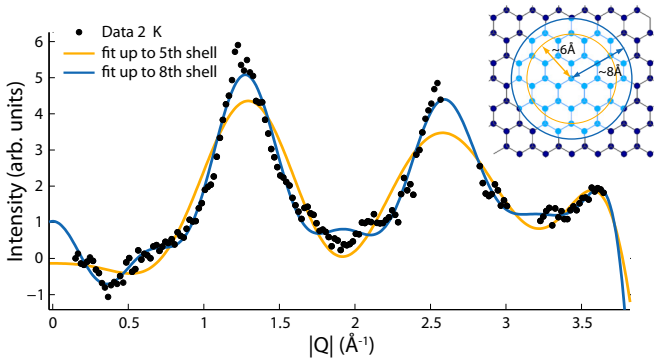

FIG. 4. Powder-averaged elastic neutron data for $LuCoGaO_4$ at $T = 1.8$ K as measured on CNCS with $E_i = 10$ meV. Fits to Eq. (1) show good agreement with short-range, two-dimensional magnetic correlations extending beyond the fifth-nearest-neighbor shell at ∼6 Å. The best fit to the data is obtained including magnetic correlations extending up to the eighth-nearest-neighbor shell at ∼8 Å, fully consistent with the correlation length determined from the line shape analysis in Fig. 3. A high-temperature, 300 K data set has been subtracted from the data as paramagnetic background, and scattering from the sample holder at $Q \sim 2.7$ and ∼3.15 $Å^{-1}$ has been excluded from the data and fit. The top-right figure illustrates how the magnetic correlations are built up in the quasi-two-dimensional shell model [16].

These independent measurements are consistent and reveal qualitatively similar behavior, showing a strong buildup of the magnetic correlations below 100 K and a rather gradual increase of the correlation length from 30 K towards its saturation value of $\xi \sim 6.5$–7.5 Å below the freezing temperature $T_g \sim 19$ K (indicated by an arrow in Fig. 3). This correlation length implies a correlated region of spins of ∼16 Å or roughly five unit cells. It is noteworthy that no sharp anomaly is observed at T_g, in contrast to the ZFC/FC susceptibility, which displays a clear cusp at the freezing temperature. This feature appears to be common to all spin-glass materials in this family.

An alternative method of extracting an approximate correlation length was proposed by Wiedenmann *et al.* who fitted powder neutron data of $LuFeMgO_4$ to a model of short-range, quasi-two-dimensional correlations using the following expression for the scattering intensity $I(Q)$: [16]

$$I(Q) \propto f^2(Q) \times \sum_l c_l \left[a_l \frac{\sin(Qr_l)}{Qr_l} + b_l \left(\frac{\sin(Qr_l)}{(Qr_l)^3} - \frac{\cos(Qr_l)}{(Qr_l)^2} \right) \right], \quad (1)$$

where $f^2(Q)$ is the magnetic form factor, c_l is the number of spins connected to a given spin l at distance r_l, and the a_l and b_l are coefficients capturing correlations between spins.

In this model, spin correlations build up for successive nearest-neighbor shells within the triangular bilayer, assuming that no correlations between adjacent bilayers are formed. The fitting results to Eq. (1) for powder-averaged CNCS data at 1.8 K using $E_i = 10$ meV are shown in Fig. 4 for correlations within two shell radii, $r_5 = 5.89$ Å and $r_8 = 8.21$ Å (see small figure on top right of Fig. 4). The data are best described by including spins correlated at distances up to the eighth-neighbor shell at ∼8 Å, which is fully consistent with the above determined correlation length of ∼7.5 Å at 1.8 K. We note here that including correlations beyond the eighth-neighbor shell does not improve the fit any further.

This observation is similar to the result reported for powder samples of $LuFeMgO_4$, for which the short-range magnetic correlations observed as diffuse scattering intensity at $|Q| \sim 1.25$ $Å^{-1}$ have been described within the above model by including correlations up to the 12th-neighbor shell, indicating a somewhat larger correlation length in this compound [16]. In the case of $LuCuGaO_4$, in which broad and extremely weak magnetic diffuse scattering at $|Q| \sim 1.2$ $Å^{-1}$ is observed in a polarized neutron diffraction experiment below temperatures ∼50 K, correlations involving only near-neighbor shells have been inferred [28]. Thus, the magnetic correlations in all members of this family so far studied are very short ranged, consistent with the experimental observations of the $|Q|$-dependent magnetic diffuse scattering.

The spin freezing process can be characterized by examining the energy dependence of the diffuse scattering peaks at low energies. For that purpose, we have taken cuts in energy through the diffuse peaks in our high-resolution CNCS data ($E_i = 10$ meV) by integrating in $[H,H,0] = [-0.5,-0.16]$ and $L = [-0.5,0.5]$ r.l.u. Fits to a Lorentzian line shape did not prove to be useful due to a small temperature-independent quasielastic feature at ∼0.8 meV that did not reproduce in

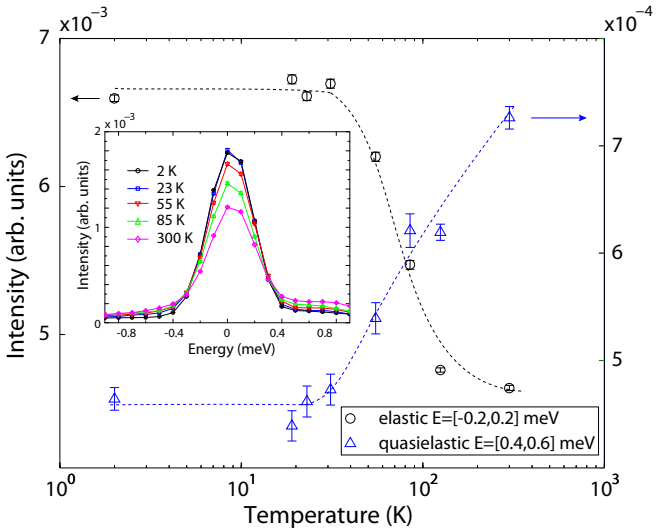

FIG. 5. Energy dependence of the diffuse scattering as measured on CNCS with $E_i = 10$ meV, integrated in $[H,H,0] = [-0.5,-0.16]$ and $L = [-0.5,0.5]$ r.l.u.. The temperature evolution of the scattering intensity at the elastic line $-0.2 < E < 0.2$ meV is contrasted to that at low inelastic energy transfers ($0.4 < E < 0.6$ meV). The observed behavior is consistent with a continuous freezing process on cooling and slowly fluctuating spin correlations that freeze out below $\sim T_g$. The inset shows representative energy cuts of the scattering. Error bars are $\pm 1\sigma$.

higher-resolution scans with $E_i = 2.5$ meV, so we parametrize the energy dependence by looking at the evolution of the scattering intensities at the elastic ($-0.2 < E < 0.2$ meV) and the low-energy quasielastic ($0.4 < E < 0.6$ meV) positions. The results are shown in Fig. 5. One can clearly see the buildup of scattering intensity at the elastic position over a wide range of temperatures that reaches a constant value below $\sim T_g$. Simultaneously, the weaker quasielastic scattering reveals a gradual decrease in intensity as the system is cooled down to $\sim T_g$. Both the buildup of the elastic scattering and the simultaneous decrease in the quasielastic scattering intensity are associated with the freezing of spin fluctuations. This is shown in the inset of Fig. 5 for a subset of scans at representative temperatures. The fact that this scattering does not change below $\sim T_g$ and that the peaks appear resolution limited in energy furthermore indicates that the spins are frozen on the time scale of this measurement, $\sim\tau \leqslant 10^{-10}$ s, at temperatures below T_g. This slowing down of spin fluctuations over a wide range of temperatures is typical of conventional spin-glass behavior [36].

IV. DYNAMIC SPIN CORRELATIONS

Modern time-of-flight neutron scattering techniques allow us to study the inelastic scattering spectrum of $LuCoGaO_4$ over a wide range of energies and wave vectors. To our knowledge, among this family of $LuM^{2+}M^{3+}O_4$, only the magnetically ordered $LuFe_2O_4$ [39] (single crystal) and the spin-liquid material $LuCuGaO_4$ [28] (powder) have been investigated in detail by inelastic neutron scattering over a wide range of $\mathbf{Q}$-E space.

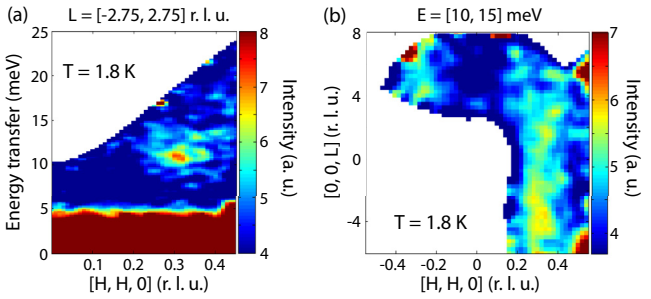

FIG. 6. Two-dimensional resonant spin excitation observed on SEQUOIA at 1.8 K. (a) Inelastic scattering integrated over $L = [-2.75,2.75]$ and $[H,-H,0] = [-0.2,0.2]$ r.l.u. is shown. A gapped spin excitation positioned at $\mathbf{Q} = (1/3,1/3,L)$ is observed at $\sim$12 meV. It has a bandwidth of $\sim$8 meV. (b) Constant energy slice within the $[H,H,L]$ scattering plane, integrated from $E = [10,15]$ meV. The resonant spin excitation is well localized at $\mathbf{Q} = (1/3,1/3,L)$ and has a clear two-dimensional, rodlike character. Its $\mathbf{Q}$ width is comparable to the width of the diffuse elastic scattering.

The magnetic excitation spectrum of $LuCoGaO_4$ at 1.8 K using SEQUOIA is shown in Fig. 6(a) for scattering as a function of momentum along $[H,H,0]$. For this measurement, we integrated over $L = [-2.75,2.75]$ and

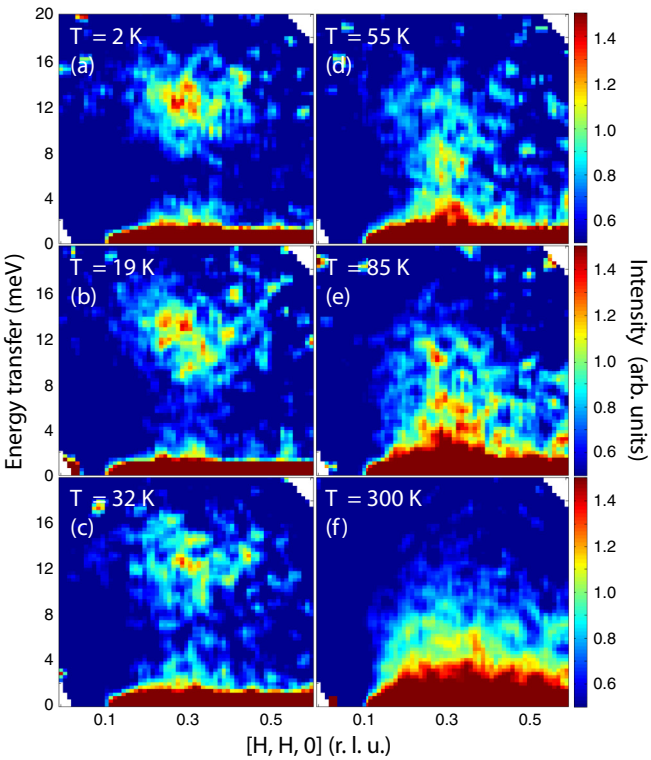

FIG. 7. Temperature evolution of the resonant spin excitation as measured on CNCS. Inelastic scattering intensity for an integration range of $L = [-2,12]$ r.l.u. and $[H,-H,0] = [-0.2,0.2]$ r.l.u. is shown for (a), $T = 2$ K, (b) $T = 19$ K, (c) $T = 32$ K, (d) $T = 55$ K, (e) $T = 85$ K, and (f) $T = 300$ K. A spin gap of $\sim$9 meV gradually opens below $\sim$85 K and is fully developed below the freezing temperature $T_g \sim 19$ K. The gap correlates with the short-range static spin correlations shown as in Figs. 2 and 3. Note that the data have only been corrected for detector efficiency.

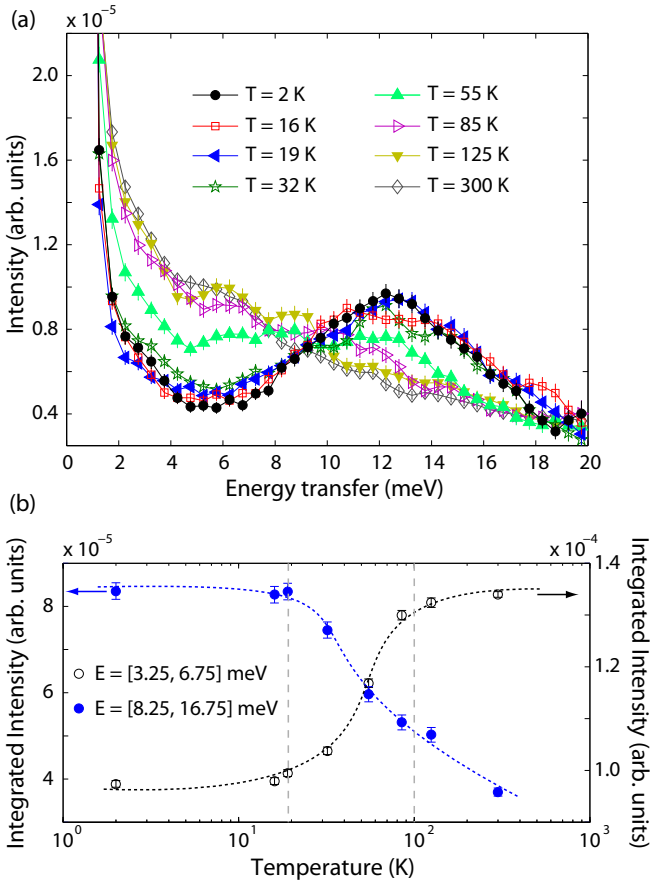

FIG. 8. (a) Neutron scattering intensity vs energy transfer for various temperatures shown for $[0,0,L] = [-2,12]$ r.l.u. and $[H,H,0] = [0.1,0.5]$ r.l.u., using the $E_i = 25$ meV data from CNCS. (b) Temperature dependence of the integrated scattering intensity associated with the formation of the spin gap at $E = [3.25,6.75]$ meV (black curve), and integrated intensity at the resonant excitation energy $E = [8.25,16.75]$ meV (blue curve), are shown to characterize the magnetic excitation in Fig. 7. The spin gap and the related spin excitation at 12 meV start to form below $|\Theta_{CW}| \sim 85$ K and appear to be fully developed below T_g, consistent with the evolution of the static spin correlations. Lines are guides to the eye.

$[H,-H,0] = [-0.2,0.2]$ r.l.u.. We clearly observe a resonant magnetic excitation that appears at wave vector $\mathbf{Q} = (1/3,1/3,L)$ centered an energy transfer of ~12 meV, gapped by ~9 meV from the elastic line. The excitation has a large bandwidth of ~8 meV and displays little dispersion. Figure 6(b) shows a constant energy slice within the (H,H,L) plane for $[H,-H,0] = [-0.2,0.2]$ r.l.u. and $E = [10,15]$ meV that reveals the two-dimensional character of this excitation. It appears as an inelastic rod of scattering along the $[0,0,L]$ direction at both $\mathbf{Q} = (-1/3,-1/3,L)$ and $\mathbf{Q} = (1/3,1/3,L)$.

We present the temperature evolution of this scattering as observed on CNCS using $E_i = 25$ meV in Fig. 7. With increasing temperature, the excitation is fairly temperature independent up to ~32 K and then starts to soften at a temperature scale $\sim\Theta_{CW}/2$. It collapses by ~85 K at the wave vector $\mathbf{Q} = (1/3,1/3,L)$. We present cuts through this inelastic spectrum in Fig. 8(a), top panel. In Fig. 8(b), bottom panel, we show the temperature dependence of integrated intensities at two different energy transfers that characterize the evolution of the scattering within the gap ($E = [3.25,6.75]$ meV) and the buildup of the magnetic excitation at 12 meV ($E = [8.25,16.75]$ meV).

The behavior of this resonant excitation clearly correlates with the development of the static correlations, as shown in Fig. 3. An onset of the static (short-range diffuse scattering) and dynamic correlations (resonant spin excitation) is observed at relatively high temperatures just around Θ_{CW}, followed by a dramatic buildup in correlations down to temperatures in the vicinity of the freezing temperature T_g at 19 K, below which both static and dynamic correlations are fully developed.

The observation of such a localized (in energy and wave vector) excitation at relatively large energy transfers raises the question about its origin. Its most natural explanation is that it arises due to the splitting of the $S_{eff} = 1/2$ Kramer's ground-state doublet of the Co^{2+} ion in a staggered mean exchange field. The mean exchange field correlates with the buildup of static spin correlations below Θ_{CW}, and the fact that it is centered on the $\mathbf{Q} = (1/3,1/3,L)$ quasiordering wave vector is indicative of the role the staggered mean exchange field plays; it is not a single-ion effect.

V. CONCLUSION

We performed the first time-of-flight neutron scattering measurements on the triangular bilayer spin glass $LuCoGaO_4$ in single-crystal form, over a wide range of temperatures in zero field. We observe diffuse elastic scattering at wave vectors $\mathbf{Q} = (1/3,1/3,L)$ that appears as rods of scattering along the c^* direction. This is consistent with short-range antiferromagnetic correlations with a correlation length $\xi \sim 6.5$–7.5 Å within decoupled bilayers in the a^*-b^* plane, confirming the two-dimensional character of this system. The energy dependence of this diffuse scattering exhibits slowing down of the spin fluctuations in a manner consistent with a typical spin-glass freezing process. These features are consistent with expectations for a conventional two-dimensional spin glass. In addition, we observe a novel magnetic excitation, which consists of a well-localized, resonant gapped ~12 meV spin excitation in our inelastic neutron scattering data. We attribute this excitation to the splitting of the $S_{eff} = 1/2$ Kramer's doublet ground state of Co^{2+} in the presence of a staggered mean exchange field. Appropriately, this resonant excitation softens in energy on the temperature scale of $|\Theta_{CW}|$, at which point the static correlations giving rise to the mean exchange field have melted away.

ACKNOWLEDGMENTS

Work at McMaster University was supported by NSERC of Canada. The research at Oak Ridge National Laboratory's Spallation Neutron Source was sponsored by the Scientific User Facilities Division, Office of Basic Energy Sciences, U.S. Department of Energy. The data were reduced using Mantid [40] and analyzed using the HORACE software package [41]. The powder average of the single-crystal data was performed in the DAVE software package [42].

[1] C. Lacroix, P. Mendels, and F. Mila, *Introduction to Frustrated Magnetism* (Springer, Heidelberg, 2011).

[2] L. Balents, Nature (London) **464**, 199 (2010).

[3] S. Nakatsuji, Y. Nambu, H. Tonomura, O. Sakai, S. Jonas, C. Broholm, H. Tsunetsugu, Y. Qiu, and Y. Maeno, Science **309**, 1697 (2005).

[4] R. Coldea, D. A. Tennant, and Z. Tylczynski, Phys. Rev. B **68**, 134424 (2003).

[5] R. Coldea, D. A. Tennant, A. M. Tsvelik, and Z. Tylczynski, Phys. Rev. Lett. **86**, 1335 (2001).

[6] S. Nakatsuji, K. Kuga, K. Kimura, R. Satake, N. Katayama, E. Nishibori, H. Sawa, R. Ishii, M. Hagiwara, F. Bridges, T. U. Ito, W. Higemoto, Y. Karaki, M. Halim, A. A. Nugroho, J. A. Rodriguez-Rivera, M. A. Green, and C. Broholm, Science **336**, 559 (2012).

[7] Y. Shimizu, K. Miyagawa, K. Kanoda, M. Maesato, and G. Saito, Phys. Rev. Lett. **91**, 107001 (2003).

[8] J. S. Helton, K. Matan, M. P. Shores, E. A. Nytko, B. M. Bartlett, Y. Yoshida, Y. Takano, A. Suslov, Y. Qiu, J.-H. Chung, D. G. Nocera, and Y. S. Lee, Phys. Rev. Lett. **98**, 107204 (2007).

[9] Y. Li, G. Chen, W. Tong, L. Pi, J. Liu, Z. Yang, X. Wang, and Q. Zhang, Phys. Rev. Lett. **115**, 167203 (2015).

[10] J. A. M. Paddison, M. Daum, Z. Dun, G. Ehlers, Y. Liu, M. B. Stone, H. Zhou, and M. Mourigal, Nat. Phys. **13**, 117 (2017).

[11] Y. Shen, Y.-D. Li, H. Wo, Y. Li, S. Shen, B. Pan, Q. Wang, H. C. Walker, P. Steffens, M. Boehm, Y. Hao, D. L. Quintero-Castro, L. W. Harriger, M. D. Frontzek, L. Hao, S. Meng, Q. Zhang, G. Chen, and J. Zhao, Nature (London) **540**, 559 (2016).

[12] R. Cava, A. Ramirez, Q. Huang, and J. Krajewski, J. Solid State Chem. **140**, 337 (1998).

[13] S. Katano, T. Matsumoto, S. Funahashi, J. Iida, M. Tanaka, and J. Cable, Physica B: Condens. Matter **213**, 218 (1995).

[14] K. Yoshii, N. Ikeda, Y. Matsuo, Y. Horibe, and S. Mori, Phys. Rev. B **76**, 024423 (2007).

[15] K. Yoshii, N. Ikeda, Y. Okajima, Y. Yoneda, Y. Matsuo, Y. Horibe, and S. Mori, Inorg. Chem. **47**, 6493 (2008).

[16] A. Wiedenmann, W. Gunsser, J. Rossat-Mignod, and M. Evrard, J. Magn. Magn. Mater. **31-34**, 1442 (1983).

[17] N. Ikeda, K. Kohn, E. Himoto, and M. Tanaka, J. Phys. Soc. Jpn. **64**, 4371 (1995).

[18] M. Tanaka, E. Himoto, and Y. Todate, J. Phys. Soc. Jpn. **64**, 2621 (1995).

[19] M. Tanaka, H. Iwasaki, K. Siratori, and I. Shindo, J. Phys. Soc. Jpn. **58**, 1433 (1989).

[20] Y. Todate, C. Kikuta, E. Himoto, M. Tanaka, and J. Suzuki, J. Phys.: Condens. Matter **10**, 4057 (1998).

[21] Y. Todate, E. Himoto, C. Kikuta, M. Tanaka, and J. Suzuki, Phys. Rev. B **57**, 485 (1998).

[22] H. A. Dabkowska, A. Dabkowski, G. M. Luke, and B. D. Gaulin, J. Cryst. Growth **234**, 411 (2002).

[23] R. Szymczak, H. A. Dabkowska, A. Dabkowski, G. M. Luke, P. Aleshkevych, J. Fink-Finowicki, and H. Szymczak, J. Phys.: Conf. Series **303**, 012064 (2011).

[24] J. Iida, M. Tanaka, Y. Nakagawa, S. Funahashi, N. Kimizuka, and S. Takekawa, J. Phys. Soc. Jpn. **62**, 1723 (1993).

[25] A. D. Christianson, M. D. Lumsden, M. Angst, Z. Yamani, W. Tian, R. Jin, E. A. Payzant, S. E. Nagler, B. C. Sales, and D. Mandrus, Phys. Rev. Lett. **100**, 107601 (2008).

[26] N. Ikeda, H. Ohsumi, K. Ohwada, K. Ishii, T. Inami, K. Kakurai, Y. Murakami, K. Yoshii, S. Mori, Y. Horibe *et al.*, Nature (London) **436**, 1136 (2005).

[27] T. Sunaga, M. Tanaka, N. Sakai, and Y. Tsunoda, J. Phys. Soc. Jpn. **70**, 3713 (2001).

[28] S. Calder, S. R. Giblin, D. R. Parker, P. P. Deen, C. Ritter, J. R. Stewart, S. Rols, and T. Fennell, J. Phys.: Condens. Matter **25**, 356002 (2013).

[29] I. Radelytskyi, R. Szymczak, H. Dabkowska, H. Noad, P. Aleshkevych, and H. Szymczak, Acta Phys. Pol. A **126**, 230 (2014).

[30] H. M. L. Noad, H. A. Dabkowska, and G. M. Luke (unpublished).

[31] M. F. Sykes and J. W. Essam, J. Math. Phys. **5**, 1117 (1964).

[32] S. E. Nagler, W. J. L. Buyers, R. L. Armstrong, and B. Briat, Phys. Rev. B **27**, 1784 (1983).

[33] H. D. Zhou, C. Xu, A. M. Hallas, H. J. Silverstein, C. R. Wiebe, I. Umegaki, J. Q. Yan, T. P. Murphy, J.-H. Park, Y. Qiu, J. R. D. Copley, J. S. Gardner, and Y. Takano, Phys. Rev. Lett. **109**, 267206 (2012).

[34] K. Fritsch, G. Ehlers, K. C. Rule, K. Habicht, M. Ramazanoglu, H. A. Dabkowska, and B. D. Gaulin, Phys. Rev. B **92**, 180404 (2015).

[35] K. A. Ross, J. W. Krizan, J. A. Rodriguez-Rivera, R. J. Cava, and C. L. Broholm, Phys. Rev. B **93**, 014433 (2016).

[36] J. A. Mydosh, *Spin Glasses: An Experimental Introduction* (CRC Press, Bristol, 1993).

[37] H. A. Dabkowska and A. B. Dabkowski, in *Handbook of Crystal Growth, Defects and Characterization* (Springer, Berlin, 2010), pp. 367–392.

[38] M. B. Stone, J. L. Niedziela, D. L. Abernathy, L. DeBeer-Schmitt, G. Ehlers, O. Garlea, G. E. Granroth, M. Graves-Brook, A. I. Kolesnikov, A. Podlesnyak, and B. Winn, Rev. Sci. Instrum. **85**, 045113 (2014).

[39] H. J. Lewtas, Ph.D. thesis, Oxford University, 2010.

[40] O. Arnold, J. Bilheux, J. Borreguero, A. Buts, S. Campbell, L. Chapon, M. Doucet, N. Draper, R. F. Leal, M. Gigg, V. Lynch, A. Markvardsen, D. Mikkelson, R. Mikkelson, R. Miller, K. Palmen, P. Parker, G. Passos, T. Perring, P. Peterson, S. Ren, M. Reuter, A. Savici, J. Taylor, R. Taylor, R. Tolchenov, W. Zhou, and J. Zikovsky, Nucl. Instrum. Methods Phys. Res. A **764**, 156 (2014).

[41] R. Ewings, A. Buts, M. Le, J. van Duijn, I. Bustinduy, and T. Perring, Nucl. Instrum. Methods Phys. Res. A **834**, 132 (2016).

[42] R. T. Azuah, L. R. Kneller, Y. Qiu, P. L. W. Tregenna-Piggott, C. M. Brown, J. R. D. Copley, and R. M. Dimeo, J. Res. Natl. Inst. Stan. Technol. **114**, 341 (2009).